Conformational Asymmetry and Quasicrystal Approximants in Linear Diblock Copolymers

Morgan W. Schulze, Ronald M. Lewis, III, James H. Lettow, Robert J. Hickey, Timothy M. Gillard, Marc A. Hillmyer, and Frank S. Bates

Phys. Rev. Lett. **118**, 207801 — Published 16 May 2017

DOI: 10.1103/PhysRevLett.118.207801

Conformational Asymmetry and Quasicrystal Approximants in Linear Diblock Copolymers

Morgan W. Schulze,[†] Ronald M. Lewis, III,[†] James H. Lettow,[†] Robert J. Hickey,[†]
Timothy M. Gillard,[†] Marc A. Hillmyer, [‡] and Frank S. Bates[†,*]

[†]*Department of Chemical Engineering and Materials Science and*

[‡]*Department of Chemistry, University of Minnesota, Minneapolis, Minnesota 55455-0431*

ABSTRACT: Small angle x-ray scattering experiments on three model low molar mass diblock copolymer systems containing minority polylactide and majority hydrocarbon blocks demonstrate that conformational asymmetry stabilizes the Frank-Kasper σ phase. Differences in block flexibility compete with space filling at constant density inducing the formation of polyhedral shaped particles that assemble into this low symmetry ordered state with local tetrahedral coordination. These results confirm predictions from self-consistent field theory that establish the origins of symmetry breaking in the ordering of block polymer melts subjected to compositional and conformational asymmetry.

Frank and Kasper postulated in their seminal publications [1,2] the existence of complex metal alloy structures constructed using tetrahedral groupings of atoms based purely on geometrical arguments for spherical packing, deriving a distinct set of Z12, Z14, Z15, and Z16 triangulated coordination polyhedra required to tile three-dimensional space. As a notable consequence of these geometric constructions, the so-called Frank-Kasper (FK) phases are often found in close proximity to quasicrystals – aperiodic arrangements characterized by rotational symmetry. Such intricate periodic crystalline and aperiodic quasicrystalline order has sporadically emerged through serendipitous discovery in a host of soft matter systems, including supramolecular assemblies [3-7], surfactants [8-10], and block polymers [11-15], underscoring the universality of space-filling and particle packing in condensed matter. However, a key outstanding challenge is to connect the origins of quasicrystal stability and corresponding

periodic approximants to the intrinsic molecular structure and intermolecular interactions in soft materials.

Block polymers are a class of macromolecules that covalently connect chemically distinct polymer blocks, each a chain of identical monomers. The simplest and most studied molecular architecture, the linear AB diblock copolymer, affords exceptional control over domain geometry, length-scale, and dynamics, through two tunable parameters: the composition $f_A = N_A/N$ and the product variable χN, where N_A and N are the normalized volumetric degrees of polymerization of the A block and the entire molecule, respectively, and χ ($\sim T^{-1}$) is the segment-segment interaction parameter. In the limits $f_A << 1/2$ and $>> 1/2$, flexible diblock copolymers form nominally spherical micelles that order on a lattice when cooled below the order-disorder transition temperature (T_{ODT}). Recent discovery of the FK σ phase [11,12] and the associated dodecagonal quasicrystalline (DDQC) state [13] in short poly(isoprene)-*b*-poly((±)-lactide) (PI–PLA) diblock copolymers has disrupted the long-standing principles of diblock copolymer phase behavior derived from numerous experiments and predictive self-consistent mean field theory (SCFT). Although theoretical insights [16,17] have implicated conformational asymmetry as an underlying parameter in the formation of FK phases in diblock and branched block polymers, these predictions have not been tested. In this Letter, we demonstrate that conformational asymmetry indeed drives the symmetry breaking required to form complex FK mesophases.

Conformational asymmetry accounts for differences in the volume pervaded by different flexible Gaussian chains as characterized by the unperturbed radius of gyration $R_g^2 = b^2(N/6)$, where b refers to the statistical segment length associated with N repeat units defined by a specific segment volume (v). The influence of conformational asymmetry on spherical packing is largely associated with the entropic penalty for chain stretching that increases interfacial curvature at fixed composition [18,19]. Broken conformational symmetry, $\varepsilon = (b_A/b_B)^2 > 1$, skews the diblock copolymer phase diagram, enlarging the sphere-forming window for $f_A < ½$. Concurrently, at sufficiently large values of ε and χN certain FK phases including σ and A15 become stable within the framework of mean-field theory [16,17]. In this work, three model

diblock copolymers that form structural analogues containing varied conformational asymmetry via simple substitutions of the hydrocarbon block were studied: poly(ethylene-*alt*-propylene)-*b*-poly((±)-lactide) (PEP–PLA) and poly(ethylethylene)-*b*-poly((±)-lactide) (PEE–PLA), in addition to PI-PLA (see Fig. 1). The designed systems span a relatively wide range of ε with similar values of N and χ. For PEP–PLA (ε = 1.06), the two blocks fill space nearly symmetrically, while substituting PEP with smaller statistical segment length blocks PI (ε = 1.32) and PEE (ε = 1.68) increases the degree of conformational asymmetry; specification of the individual statistical segment lengths is derived from an imperfect but convenient treatment of short diblocks as random coils and is provided in the Supplemental Material [20].

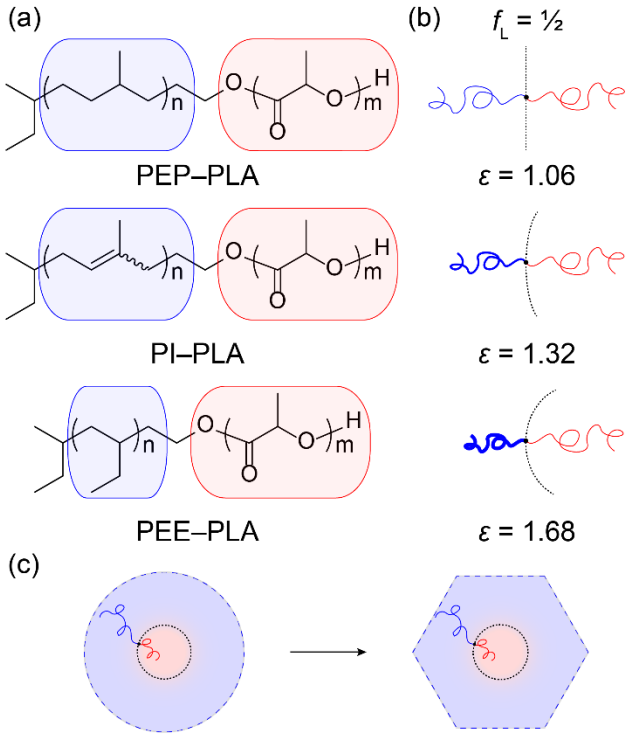

FIG. 1. (a) Molecular structure and (b) schematic representation of PEP–PLA, PI–PLA, and PEE–PLA diblock copolymers. The thickness and length of each block in (b) represent a common molecular volume (f_L = ½) to accentuate the differences in space-filling characteristics imaged in cross-section (~R_g^2). For PEP–PLA (ε = 1.06), the blocks fill space symmetrically. However, for PI–PLA (ε = 1.32) and PEE–PLA (ε = 1.68), conformational asymmetry becomes increasingly apparent, driving concave interfacial curvature toward the PLA block. (c) Depiction of a spherical micelle and the resulting polyhedral shaped domain associated with the ordered structure of

compositionally asymmetric diblocks [13].

We synthesized a series of PEP–PLA, PI–PLA, and PEE–PLA polymers with low molar mass dispersity ($Đ < 1.1$) and $f_L \leq 0.37$ using established procedures (see Supplemental Material [20], section on Materials). Order-disorder transition temperatures (T_{ODT}'s) were positioned within the experimentally accessible temperature window $T_{g,L} < T < 200$ °C, where $T_{g,L}$ is the glass transition temperature of the PLA block, which lies far above that of the majority hydrocarbon blocks (Supplemental Material, Tables S1–3 [20]). Dynamic mechanical thermal analysis (DMTA) was used to measure the T_{ODT} of each sample by monitoring the dynamic elastic shear modulus on slow heating (1–2 °C/min) at a fixed low frequency. The interaction parameters $\chi = \alpha/T + \beta$ for PEP-PLA [28] and PI-PLA [29] were obtained from the literature and normalized to a common segment volume of 118 Å^3. For PEE-PLA, α and β were estimated using a series of compositionally symmetric samples ($f_L = 0.5$) and the associated order-disorder transition temperatures (T_{ODT}'s) under the mean-field assumption $(\chi N)_{ODT} = 10.5$ [20]. Small-angle X-ray scattering (SAXS) experiments, conducted at the Advanced Photon Source (APS) at Argonne National Laboratory, were used to identify the T_{ODT} and establish ordered-state symmetries as a function of temperature and thermal history. Scattering patterns were recorded on an area detector and reduced to the 1-dimensional form of relative intensity versus the magnitude of the scattering wave vector, $q = 4\pi\lambda^{-1}\sin(\theta/2)$, where λ is the radiation wavelength and θ is the scattering angle.

The phase portraits constructed for each block polymer map the equilibrium morphologies onto the coordinates χN and f_L using χ(T) as shown in Fig. 2. Three ordered structures (BCC, the FK σ phase, and hexagonally-close packed cylinders (HEX)) and the disordered state (DIS) were identified within the compositional windows explored. Mesoscopic assemblies of monodisperse asymmetric diblock copolymer micelles have been predicted [30] and observed [31] to order on a body-centered cubic (BCC) lattice, forming polyhedral "particles" that compose the Wigner-Seitz cells (Fig. 1(c)). Nearly conformationally symmetric PEP–PLA ($\varepsilon = 1.06$) exhibits only the

HEX and BCC morphologies in the composition range $f_L < 0.32$, a refinement of the phase portrait reported by Schmidt and Hillmyer [28]. Modestly asymmetric PI–PLA ($\varepsilon = 1.32$) displays a stable σ phase window bordered by these classical phases. This system undergoes a σ-to-BCC phase transition that requires mass exchange mediated redistribution of the single type of truncated octahedron associated with the BCC state to a collection of five different polyhedra (30 in total per unit cell) of the σ phase that on average better approximate spherical symmetry [11]. Increasing statistical segment length asymmetry to $\varepsilon = 1.68$ leads to a direct window from the DIS state to the σ phase in the PEE-PLA phase diagram. Notably, the theoretical phase portrait [17] does not account for a direct transition across a σ-DIS phase boundary even for $\varepsilon = 4.0$. This discrepancy can be attributed to the mean-field picture ($N \rightarrow \infty$) of the homogeneous disordered state [29]. The presence of composition fluctuations in the exceptionally low molar mass materials used in the present study, $N < 100$, leads to a liquid-like arrangement of micelles, which increases $(\chi N)_{ODT}$, effectively "cutting-off" the BCC window adjacent to the disordered phase. The invariant degree of polymerization $\bar{N} = Nb^6/v^2$, which controls the magnitude of the fluctuation effects [32,33], varies over a relatively narrow range of 130–510 (see Supplemental Material [20]).

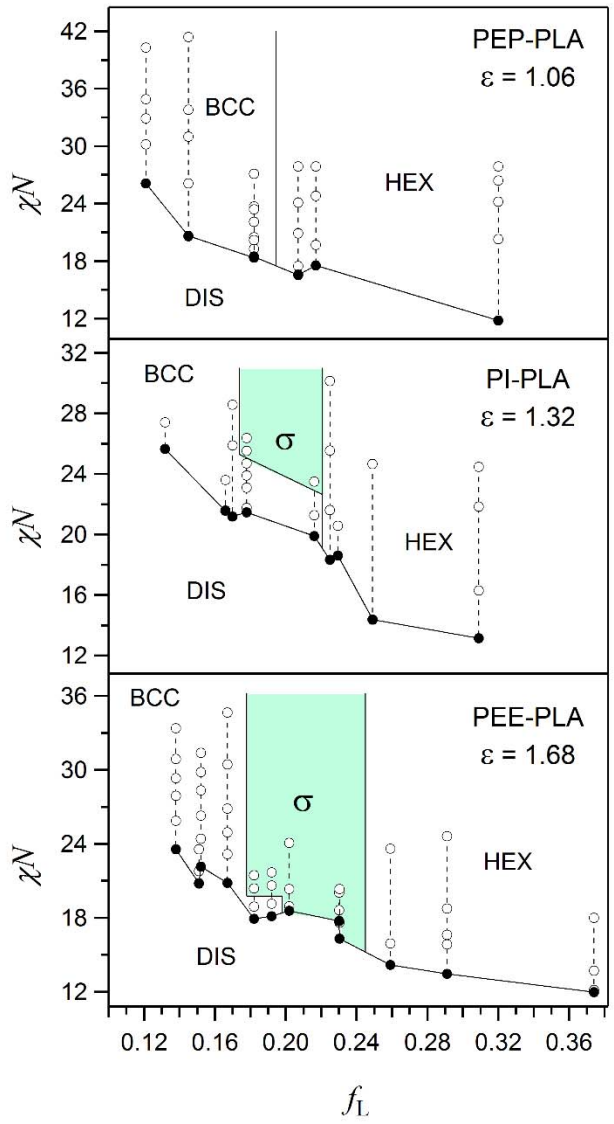

FIG. 2. Experimental phase portraits for compositionally asymmetric PEP–PLA, PI–PLA, and PEE–PLA block polymers. Points examined by SAXS are marked by white circles (○) and $(\chi N)_{ODT}$ identified by DMTA based on the mean-field theory is indicated by black circles (●). The behavior of the PI-PLA samples has been previously reported [11-13,29,34].

Fig. 3 contains a representative example of the direct σ-to-DIS transition unique to PEE–PLA as observed via SAXS for the sample denoted EL-44-23 (M_n = 3600 g/mol, $Đ$ = 1.08, f_L = 0.23). Cooling from the disordered state to 10 °C below T_{ODT} immediately produced an isotropic ring of scattered intensity, which we nominally associate with hexagonal order. Within 1 minute, a

"spotty" 2D diffraction pattern began to appear, and after 15 minutes of annealing, the isotropic ring had disappeared completely, replaced by intense discrete diffraction spots consistent with nucleation and growth of large single crystal grains of the σ phase. Subsequent heating at 1 °C/min melted the ordered σ phase at 109 °C regenerating the single broad scattering peak characteristic of the disordered state. Competitive growth of the HEX cylinder and particle based σ phases suggest two alternative nucleation mechanisms. For the development of the HEX phase, we postulate that as the system becomes unstable upon cooling below T_{ODT}, a transition involving micelle fusion rapidly nucleates numerous small grains of cylinders [35,36]. In contrast, the complex σ phase requires a cooperative organization and distribution of chains across 30 well-defined polyhedral particles such that few σ nuclei overcome the nucleation barrier despite the accelerated rate of chain exchange near T_{ODT}.

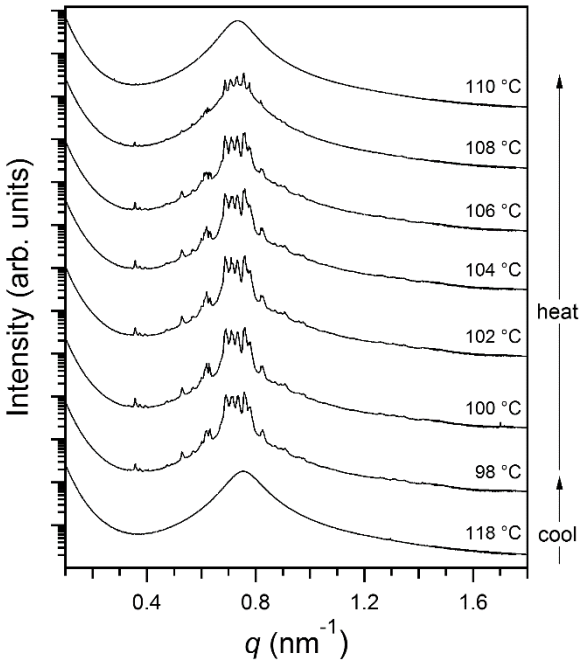

FIG. 3. Representative synchrotron SAXS data obtained from PEE–PLA (EL-44-23). A SAXS pattern consistent with the σ phase is formed upon cooling below the T_{ODT} to 98 °C and annealing for 15 min. A direct σ-to-disorder transition is observed with subsequent heating at a ramp rate of 1 °C/min. Curves are shifted vertically for clarity.

We also observed that fast (≥ 30 °C/min) temperature quenches from above T_{ODT} to between 55 and 85 °C led to the rapid development of diffraction peaks at relative positions $(q/q^*)^2 = 1, 3, 4, 7$ indicative of hexagonal symmetry (Supplemental Material [20], Fig. S2). This indicates the aforementioned micelle fusion mechanism remains active at these temperatures. Although far above the glass transition of either block, limited chain diffusion when $T << T_{ODT}$ (i.e., in strong segregation) drastically inhibits formation of the σ phase as shown previously with PI-PLA [13]. Hexagonal or coexisting hexagonal and σ phases exhibited a slow transition to the σ phase after long periods of isothermal annealing. This strong time and temperature dependent behavior was further manifested during continuous heating (Supplemental Material [20], Fig. S3(a)) or isothermal annealing at higher temperatures, which accelerated growth of the σ phase at the expense of hexagonal domains. These results are consistent with our conclusion that at equilibrium the σ phase forms a continuous channel in the phase portrait for $\chi N > (\chi N)_{ODT}$ as shown in Fig. 2.

Spontaneous formation of a metastable HEX phase upon cooling motivated experiments to probe alternative thermal processing pathways. Heating EL-44-23 above T_{ODT} and subsequent immersion in liquid nitrogen (T = –196 °C) arrested the disordered yet structured melt as a supercooled state of liquid-like packing (LLP). SAXS patterns obtained after 235 days of annealing at 20 °C showed no observable change, retaining a broad principal peak and a series of broad and weak maxima at higher values of the scattering wavevector indicative of specific short-range particle correlations (Supplemental Material [20], Fig. S4(a)). We have shown elsewhere that this supercooled disordered state exhibits features of a soft glass, kinetically trapped due to restricted chain diffusion below the ergodicity temperature, T_{erg} [13]. Heating from this initial state to 80 °C generated a dodecagonal quasicrystalline (DDQC) intermediate (Supplemental Material [20], Fig. S3(b)), mirroring the metastable DDQC state shown to slowly evolve in supercooled disordered PI–PLA [13]. Within minutes of further heating to 90 °C, the SAXS pattern developed reflections consistent with the σ phase. No further transitions were

observed by SAXS upon continued isothermal annealing. We conclude from these combined results that the σ-to-DIS transition in PEE-PLA reflects an equilibrium transition.

Absence of the σ phase in the PEP–PLA phase diagram is consistent with the theoretical prediction that significant conformational asymmetry is a prerequisite for the development of the FK phase. However, an alternative possibility is that the collection of synthesized PEP–PLA polymers lack adequate composition resolution to pinpoint a narrow window of σ phase stability between the BCC and HEX phases. To explore this, we refined this phase diagram using four binary blends of f_L = 0.18 and 0.22 PEP–PLA diblocks containing nearly equal length PEP blocks. Microstructures of the blend series were determined via SAXS using a similar protocol to that employed for the pure block polymers. These samples behaved as single-component materials with minority PLA volume fractions corresponding to the original diblocks and their proportion in the blend, retaining BCC and HEX morphologies (Fig. 4(a)). Significantly, on heating and cooling, two of the blends (f_L = 0.19 and 0.20) exhibit the sequence of phase transitions HEX ↔ BCC ↔ DIS as illustrated by the SAXS profiles found in Fig. 4(b). These results demonstrate characteristic curvature of the ordered HEX-BCC phase boundary in the vicinity of the ODT and confirm extinction of the FK σ phase in the limit $\varepsilon \leq 1.06$ over the indicated range of χN.

Although conformationally symmetric diblock copolymers are unable to form the σ phase, binary mixtures of AB diblock copolymers with substantial compositional and molar mass dispersity may lead to σ phase stability by providing a mechanism to modulate the size and shape of the constituent particles. Recent SCFT calculations [37] anticipate that larger values of dispersity of the minority component mimics conformational asymmetry via partitioning of long and short chains along the radial direction of each particle, thereby reducing the entropic penalty for chain stretching and deformation of the core. Paralleling these simulations, the blends of Fig. 4 constitute a mixture of approximately equal molar mass PEP; variation of the total chain lengths ($\gamma = N_2/N_1$) and overall compositions are controlled primarily by the PLA block. The

relative length ratio between the two diblock copolymers used here, $\gamma = 1.07$, must be smaller than the critical γ above which the σ phase is predicted to be stable.

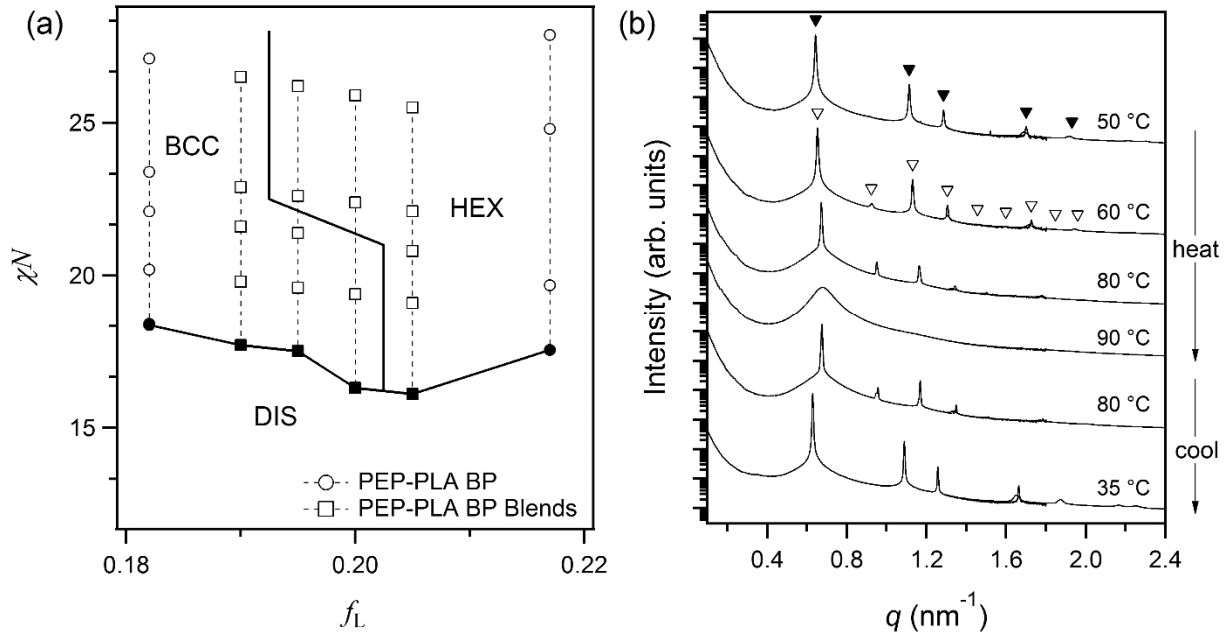

FIG. 4. (a) Experimental phase diagram for binary blends of PEP–PLA diblock copolymers centered about the BCC–HEX phase boundary. The phase space points examined by SAXS are marked by white dots and squares (○,□) for the PEP–PLA precursor block copolymers and associated blends, respectively. For blend samples, $(\chi N)_{ODT}$ is identified by SAXS based on the mean-field theory and marked by black squares (■). (b) SAXS patterns collected for a PEP–PLA blend of $f_L = 0.20$, illustrating the direct HEX-to-BCC and BCC-to-DIS transitions. The relative peak positions of the HEX phase at 50 °C, $(q/q^*)^2 = 1, 3, 4, 7, 9$ are marked by closed triangles. BCC is identified at 60 °C with $(q/q^*)^2 = 1, 2, 3, 4, 5, 6, 7, 8, 9$ (open triangles). The transition is reversible as established by subsequently cooling to 35 °C to reform the HEX structure. Curves are shifted vertically for clarity.

In contrast, we have found that substantial differences in composition and in *both* block lengths (N_{A1}/N_{A2}, N_{B1}/N_{B2}) can stabilize the σ phase (see Supplemental Material [20], Fig. S6). For PEP–PLA at a similar composition as the blends in Fig. 4 ($f_L \approx 0.20$), binary mixtures of $f_L = 0.15$ and 0.32 differing in total molar mass and both block lengths formed the σ phase after annealing for 7 days at 100 °C. Theory predicts that particle size symmetry breaking is facilitated by an inhomogeneous distribution of the two diblocks, with a higher concentration of the more

compositionally symmetric copolymer producing larger sphere volumes [37]. Preferential segregation of the two diblocks within each particle likely compounds this effect by increasing local interfacial curvature, resulting in shape regulation and non-spherical particles [37]. Collectively, our results highlight the impact of dispersity on ordered-state symmetry, experimentally validating theoretical predictions that blends afford a simple route to obtain complex FK phases.

In summary, our experimental work supports recent theoretical conclusions that conformational asymmetry underpins the formation of FK phases in block polymer materials. This effort highlights the interplay between theory and experiment in the discovery of new forms of self-assembled soft matter, ultimately catalyzing efforts to fully elucidate a parameter space that accesses new ordered-state symmetries. Linear diblock copolymers are among the simplest molecular motifs capable of generating the complex structural order characteristic of FK and quasicrystal phases in soft matter and thus serve as model systems for uncovering the origins and stability of periodic and aperiodic order. The effects that emerge with increasing conformational asymmetry in linear diblocks will be amplified by the incorporation of branching [16] and more highly asymmetric molecular constructs [7]. We expect such results to be universal, offering flexibility in the choice of block material if proper conformational parameters or molar mass dispersities are utilized in conjunction with appropriate processing conditions including annealing time and temperature.

We are grateful to Christopher M. Bates for a critical reading of our manuscript. Support for this work was provided by the National Science Foundation under award DMR-1104368 and the University of Minnesota MRSEC (DMR-1420013). Small and medium-angle X-ray scattering experiments were performed at the Advanced Photon Source (APS), Sector 5 (DuPont-Northwestern-Dow Collaborative Access Team, DND-CAT). DND-CAT is supported by E.I. DuPont de Nemours & Co., The Dow Chemical Company and Northwestern University. Use of the APS, an Office of Science User Facility operated for the U.S. Department of Energy (DOE) Office of Science by Argonne National Laboratory, was supported by the U.S. DOE under

Contract No. DE-AC02-06CH11357. Data was collected using an instrument funded by the National Science Foundation under Award Number 0960140.

---

[1] F. C. Frank and J. S. Kasper, Acta Crystallographica **11**, 184-190 (1958).

[2] F. C. Frank and J. S. Kasper, Acta Crystallographica **12**, 483-499 (1959).

[3] X. Zeng, G. Ungar, Y. Liu, V. Percec, A. E. Dulcey and J. K. Hobbs, Nature **428**, 157-160 (2004).

[4] G. Ungar and X. Zeng, Soft Matter **1**, 95-106 (2005).

[5] M. Huang, C.-H. Hsu, J. Wang, S. Mei, X. Dong, Y. Li, M. Li, H. Liu, W. Zhang, T. Aida, W.-B. Zhang, K. Yue and S. Z. D. Cheng, Science **348**, 424-428 (2015).

[6] G. Ungar, Y. Liu, X. Zeng, V. Percec and W.-D. Cho, Science **299**, 1208-1211 (2003).

[7] K. Yue, M. Huang, R. L. Marson, J. He, J. Huang, Z. Zhou, J. Wang, C. Liu, X. Yan, K. Wu, Z. Guo, H. Liu, W. Zhang, P. Ni, C. Wesdemiotis, W.-B. Zhang, S. C. Glotzer and S. Z. D. Cheng, Proceedings of the National Academy of Sciences **113**, 14195-14200 (2016).

[8] P. Sakya, J. M. Seddon, R. H. Templer, R. J. Mirkin and G. J. T. Tiddy, Langmuir **13**, 3706-3714 (1997).

[9] R. Vargas, P. Mariani, A. Gulik and V. Luzzati, Journal of Molecular Biology **225**, 137-145 (1992).

[10] S. Che, A. E. Garcia-Bennett, T. Yokoi, K. Sakamoto, H. Kunieda, O. Terasaki and T. Tatsumi, Nat Mater **2**, 801-805 (2003).

[11] S. Lee, C. Leighton and F. S. Bates, Proceedings of the National Academy of Sciences **111**, 17723-17731 (2014).

[12] S. Lee, M. J. Bluemle and F. S. Bates, Science **330**, 349-353 (2010).

[13] T. M. Gillard, S. Lee and F. S. Bates, Proceedings of the National Academy of Sciences **113**, 5167-5172 (2016).

[14] J. Zhang and F. S. Bates, Journal of the American Chemical Society **134**, 7636-7639 (2012).

[15] S. Chanpuriya, K. Kim, J. Zhang, S. Lee, A. Arora, K. D. Dorfman, K. T. Delaney, G. H. Fredrickson and F. S. Bates, ACS Nano **10**, 4961-4972 (2016).

[16] G. M. Grason, B. A. DiDonna and R. D. Kamien, Physical Review Letters **91**, 058304 (2003).

[17] N. Xie, W. Li, F. Qiu and A.-C. Shi, ACS Macro Letters **3**, 906-910 (2014).

[18] M. W. Matsen and F. S. Bates, Journal of Polymer Science Part B: Polymer Physics **35**, 945-952 (1997).

[19] J. D. Vavasour and M. D. Whitmore, Macromolecules **26**, 7070-7075 (1993).

[20] See Supplemental Material at http://link.aps.org/supplemental/10.1103/PhysRevLett.XXX.XXXXXX, which includes Refs. [21-27], details concerning experimental procedures, sample characterization, estimation of the interaction parameter and representative SAXS data.

[21] M. A. Hillmyer and F. S. Bates, Macromolecules **29**, 6994-7002 (1996).

[22] N. A. Lynd and M. A. Hillmyer, Macromolecules **38**, 8803-8810 (2005).

[23] L. J. Fetters, D. J. Lohse, D. Richter, T. A. Witten and A. Zirkel, Macromolecules **27**, 4639-4647 (1994).

[24] K. S. Anderson and M. A. Hillmyer, Macromolecules **37**, 1857-1862 (2004).

[25] D. E. Henton, P. Gruber, J. Lunt and J. Randall, in *Natural Fibers, Biopolymers, and Biocomposites*, edited by A. K. Mohanty, M. Misra and L. T. Drzal (CRC Press, New York, 2005).

[26] C. A. P. Joziasse, H. Veenstra, D. W. Grijpma and A. J. Pennings, Macromolecular Chemistry and Physics **197**, 2219-2229 (1996).

[27] K. Almdal, M. A. Hillmyer and F. S. Bates, Macromolecules **35**, 7685-7691 (2002).

[28] S. C. Schmidt and M. A. Hillmyer, Journal of Polymer Science Part B: Polymer Physics **40**, 2364-2376 (2002).

[29] S. Lee, T. M. Gillard and F. S. Bates, AIChe J **59**, 3502-3513 (2013).

[30] L. Leibler, Macromolecules **13**, 1602-1617 (1980).

[31] F. S. Bates, R. E. Cohen and C. V. Berney, Macromolecules **15**, 589-592 (1982).

[32] G. H. Fredrickson and E. Helfand, The Journal of Chemical Physics **87**, 697-705 (1987).

[33] J. Qin and D. C. Morse, Physical Review Letters **108**, 238301 (2012).

[34] T. M. Gillard, Ph.D. Thesis, University of Minneosta, 2015.

[35] K. A. Koppi, M. Tirrell, F. S. Bates, K. Almdal and K. Mortensen, Journal of Rheology **38**, 999-1027 (1994).

[36] C. Y. Ryu and T. P. Lodge, Macromolecules **32**, 7190-7201 (1999).

[37] M. Liu, Y. Qiang, W. Li, F. Qiu and A.-C. Shi, ACS Macro Letters, 1167-1171 (2016).